

## Axial and Radial Potential Structure and Current Flow in GAMMA 10

SAITO Teruo\*, CHO Teruji, HIRATA Mafumi, HOJO Hitoshi, ISHII Kameo, ICHIMURA Makoto, ITAKURA Akiyoshi, KATANUMA Isao, KOHAGURA Junko, NAKASHIMA Yousuke, TATEMATSU Yoshinori, YATSU Kiyoshi and YOSHIKAWA Masayuki  
*Plasma Research Center, University of Tsukuba, Tsukuba 305-8577, Japan*

(Received: 5 December 2000 / Accepted: 27 August 2001)

### Abstract

Tandem mirror experiments have proved generation of a plug potential and strong suppression of end loss ions has been realized. A substantial improvement of plasma confinement by potential is obtained in the GAMMA 10 tandem mirror. This paper presents experimental observations about potential formation in GAMMA 10. The plug ECRH of fundamental resonance at the plug region plays a largest role in the potential formation. On application of the plug ECRH, the axial and radial potential structures show significant changes. Since plugging reshapes the density distribution of the ions near the plug region, potential generation is a dynamic process. In addition, an intense axial flow of warm electrons driven by the plug ECRH is a key factor of the potential distribution. The potential difference between the plug and the barrier mid plane increases with the temperature of the warm electrons, while the barrier depth scales with the bulk electron temperature. The warm electron flow also connects the plug potential to the potential in the end region.

### Keywords:

tandem mirror, potential confinement, potential formation, plug potential, thermal barrier, ECRH, ambipolar potential

### 1. Introduction

Tandem mirror experiments have proved creation of a plug potential and the concept of potential confinement (plugging) is now widely accepted [1]. Along with the proof of principle study, many theoretical and experimental works have been done on the physics of potential formation. This paper presents the experimental observations about potential formation in a tandem mirror with a thermal barrier and discusses the relevant physics. Experimental data are obtained mostly from the GAMMA 10 tandem mirror [2]. GAMMA 10 experiments have shown a remarkable improvement of plasma confinement by creating a plug potential and efforts toward further improvement are under way [3].

The particle flow induced by ECRH is closely related to both potential and plasma confinement. Thus continuous efforts for understanding of the potential physics are very important.

Formation of a thermal barrier and a plug potential originally assumed a density distribution of ions as a static background [4]. Then, ECRH was supposed to act on electrons that follow the ion distribution. In GAMMA 10, the axial potential distribution strongly varies on application of fundamental ECRH at the plug region (plug ECRH) and the ion confining potential is generated. Experiments have shown the importance of an axial flow of warm electrons driven by the plug

\*Corresponding author's e-mail: [saito@prc.tsukuba.ac.jp](mailto:saito@prc.tsukuba.ac.jp)

ECRH [5]. This electron flow connects the plug region to an end region. A plasma flow emanating from the central cell is another important factor. The plug potential reshapes the density distribution of the flow plasma. Thus potential formation and plugging cannot be divided into independent processes. Recently, a new scheme has been presented on creation of the plug potential [6,7]. This scheme shows that the plug ECRH brings about an asymmetry with respect to the mid plane of an end mirror cell and a plug potential is created in the outer side of this cell. A basic experiment has shown that a plug potential can be formed by ECRH only [8,9]. ECRH causes mirror-reflection of electrons flowing out of a source region, which leads to reflection of ions by a plug potential. These new schemes provide important view points.

This paper is constructed as follows. First, a brief description is given in Sec. 2 on the evolution of the concept of potential confinement. The experimental configuration of GAMMA 10 is illustrated in Sec. 3. Then, Sec. 4 presents experimental observations. Section 5 discusses the experimental results. Finally, Sec. 6 is devoted to conclusions of this paper.

## 2. Evolution of a Tandem Mirror Concept

In this section, we briefly describe the evolution of the concept of a tandem mirror. We cite only representative papers. For a list of comprehensive references, see Ref. 10. An ambipolar potential is generated in a simple mirror plasma. The electrons are confined by this potential [11]. However, ion confinement should rely on mirror confinement, because this potential expels ions. To improve ion confinement, an idea of a tandem mirror has been presented, in which ions are also confined by a potential barrier (plug potential) [12-14]. The Boltzmann's law is assumed on electrons with an electron temperature  $T_e$  and an ion confining potential  $\phi_c = T_e \ln(n_p/n_c)$  is created in auxiliary plug cells (electron density  $n_p$ ) attached to both ends of a central cell (electron density  $n_c$ ). Electrons are confined by the ambipolar potential. The Boltzmann's law assumes a thermal plasma and is physically reliable. This idea has been proved on GAMMA 6 and TMX [15,16]. However, a tandem mirror of this type requires a very large  $n_p$ . Moreover, it requires a static density in the plug cell that is not affected by potential. This is provided by magnetically confined non-thermal energetic ions with a density corresponding to  $n_p$ .

A concept of a thermal barrier has been invented [17]. With a help of the thermal barrier, the plug potential can be realized even for  $n_p < n_c$ . Formation of

a thermal barrier and a plug potential has been shown in GAMMA 10, TMX-U and TARA [2,18,19]. This scheme of potential formation requires non-thermal electrons instead of thermal electrons. ECRH is expected to control the electron velocity distribution function [4]. Cohen *et al.* have developed theoretical models of this scheme and provided a guiding principle of experiments [20,21]. ECRH gives electrons an increment of magnetic moment and exhausts electrons from the plug region because of the  $\mu \nabla B$  force. Then an excess positive charge is left in the plug region, which results in a positive potential. This scheme also assumes a static axial ion distribution in a mirror cell in which the plug potential is formed. However, experiments indicate that ions as well as electrons respond to the potential. This is one of the main points of the present paper.

## 3. Experimental Configuration and Diagnostics

The main elements of GAMMA 10 are a central cell, two min-B anchor cells located in both ends of the central cell and two end mirror cells connected to each anchor cell. Figure 1 (a) illustrates the end mirror cell in which the plug potential is created. The magnetic field strengths at both mirror throats are 3.0T and that at the mid plane is 0.5T for a standard experiment. Plug ECRH of fundamental resonance is applied at the plug position in each end mirror cell. The magnetic field strength at the plug is 1.0T and has an axial gradient. The microwave power delivered from a 28GHz gyrotron with a maximum power of 200kW is radiated from a Vlasov antenna and injected to the resonance surface in the x-mode after reflection off a cylindrical mirror. The radiation pattern of the plug ECRH is nearly axi-symmetrized on the resonance surface [22]. Second harmonic ECRH is also carried out with another gyrotron at the mid plane of each end mirror cell. We do not consider the effect of the second harmonic ECRH in this paper.

The end region is located outside the end mirror cell in which the magnetic flux tube is expanded. An end plate of stainless steel is installed on an end wall of the vacuum vessel. The end plate is usually connected to the vacuum vessel with a high resistance and is electrically floating. End loss electrons and ions are measured with an electrostatic energy analyzer located behind a small hole of the end plate. The magnetic field strength at the end plate is 0.01T, 1/40 times as large as that at the central cell mid plane ( $B = 0.4T$ ).

Beam probes measure the potential  $\Phi_C$  near the mid plane of the central cell and the potential  $\Phi_B$  at the mid

plane of the end mirror cell [23]. The potential  $\Phi_p$  at the plug position is evaluated with an end loss analyzer [24]. Several Langmuir probes are used to measure potentials in the end region [25]. All these potentials are measured in reference to the vacuum vessel and represented by capital  $\Phi$ . Potential differences between two positions are denoted by lower case  $\phi$ .

Two ring electrodes made of stainless steel are installed in the end mirror cell. Besides these electrodes, a ring limiter is located near the inner mirror throat. The axial positions and the flux-mapped radii equivalent to the central cell mid plane are shown in Fig. 1 (b). The equivalent radii of the electrodes and the mirror throat limiter are larger than the radius 18cm of the central cell limiter. The central-cell equivalent radii of five concentric annular plates of the end plate are also shown.

#### 4. Potential Structure and Current Flow in GAMMA 10

An ICRF wave excited in the central cell sustains a plasma and a slow wave with a different frequency heats ions in the central cell [26]. After a steady state is attained, the plug ECRH is turned on to create the plug

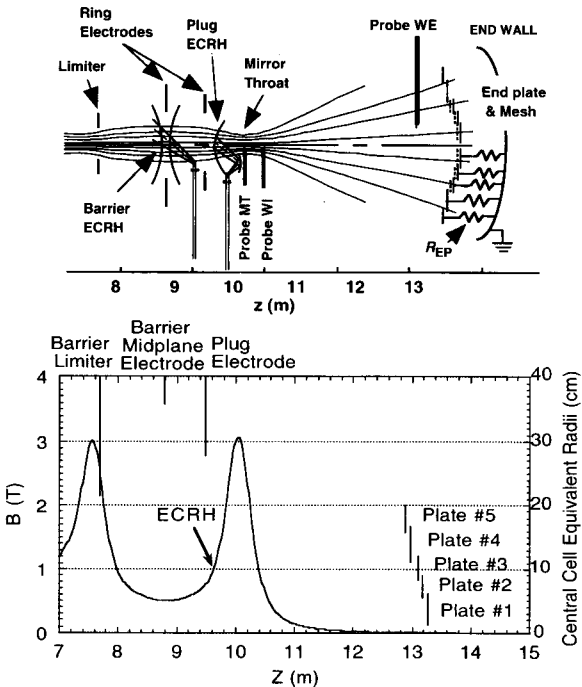


Fig. 1 The configuration of the end mirror cell and the end region of GAMMA 10 is shown in Fig. (a). Figure (b) plots the axial distribution of the magnetic field strength and the flux-mapped radii of the electrodes and the annular plates of the end plate equivalent to the central cell mid plane.

potential. Figure 2 shows wave forms of the plug potential  $\Phi_p$ , the central cell potential  $\Phi_c$ , the barrier potential  $\Phi_b$  at the mid plane of the end mirror cell and the end plate potential  $\Phi_{ep}$ . On application of the plug ECRH, potentials at each position substantially vary and  $\Phi_p$  becomes highest.

#### 4.1 Potential Structure of a Whole Plasma

Figure 3 depicts the axial profile of the potential at cardinal axial positions. The difference  $\phi_c = \Phi_p - \Phi_c$  is the ion confining potential and  $\phi_b = \Phi_c - \Phi_b$  is the thermal barrier depth. The plug ECRH rearranges the axial potential distribution and a positive ion confining potential is produced. The electron density at the plug region is one tenth of the central cell electron density at maximum but a positive  $\phi_c$  is generated. The plug ECRH also has a strong influence on the potential profile in the end region. The floating end plate potential becomes deeply negative as a result of a decrease in the potential outside of the mirror throat and a sheath potential drop in front of the end plate. The axial potential structure in the end mirror cell is discussed in Sec. 4.3. As shown below, the plug ECRH drives an intense axial flow of warm electrons and the end plate potential becomes negative with respect to the plug region from where electrons are driven out. Since detailed studies have been done on the axial potential distribution in the end region [5,25,27-31], we do not show more details of the end plate potential here.

The potentials as plotted in Fig. 3 strongly depend on the plug ECRH power. Figure 4 plots the potentials

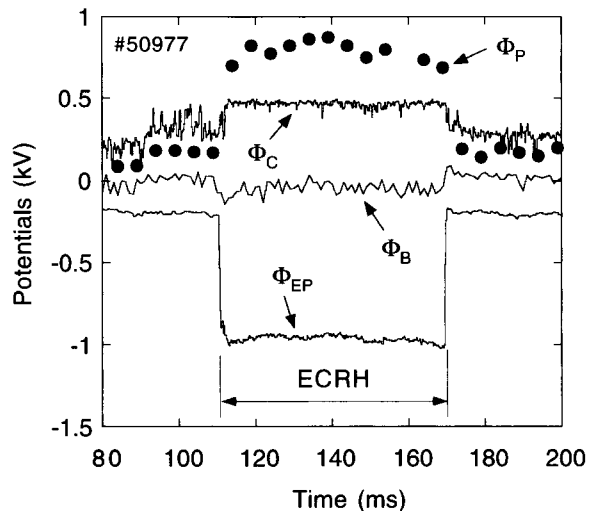


Fig. 2 Typical wave forms of the plasma potentials at cardinal positions. These potentials are measured in reference to the vacuum vessel.

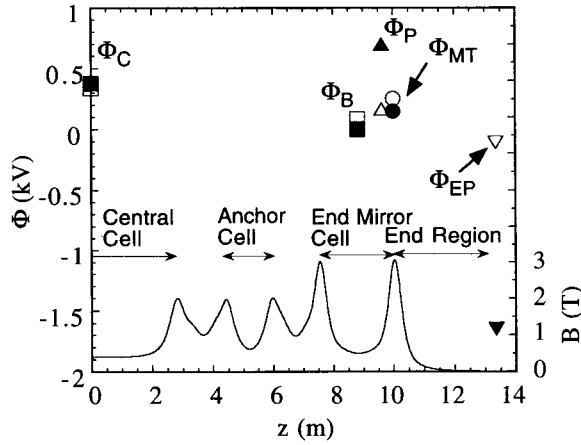


Fig. 3 Axial distributions are plotted of the potential without (open symbols) and with (closed symbols) the plug ECRH.

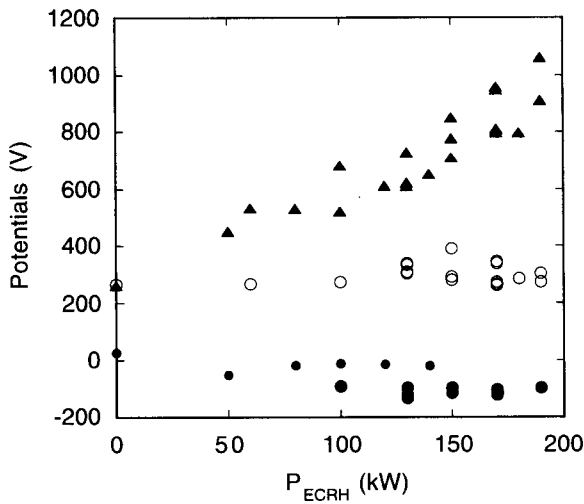


Fig. 4 The plug potential  $\Phi_p$  (upward triangle), the central cell potential  $\Phi_c$  (open circle) and the barrier mid plane potential  $\Phi_b$  (closed circle) are plotted as functions of the gyrotron power  $P_{ECRH}$  for the plug ECRH.

as functions of the gyrotron power  $P_{ECRH}$  for the plug ECRH. The value of  $\Phi_p$  increases with  $P_{ECRH}$ . On the other hand,  $\Phi_c$  increases by a small amount at a low ECRH power and a decrease in  $\Phi_b$  is also small. For higher ECRH power  $\Phi_c$  and  $\Phi_b$  do not vary very much. As a result of the increase in  $\Phi_p$ , the confining potential  $\phi_c$  attains up to 800V at  $P_{ECRH}$  of 190kW.

The radial profile of the potential is also important information. Radial profiles of the potential are available at limited positions at the moment. Figure 5 shows the radial profiles  $\Phi_p$ ,  $\Phi_c$ ,  $\Phi_b$  and  $\Phi_{WI}$ . The two-

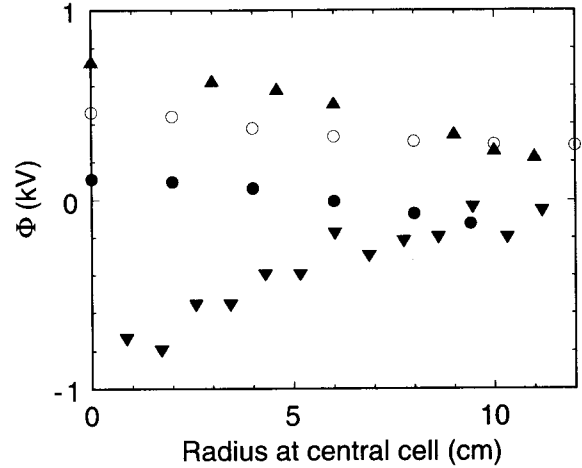


Fig. 5 The radial profiles are plotted of the plug potential  $\Phi_p$  (upward triangle), the central cell potential  $\Phi_c$  (open circle), the barrier potential  $\Phi_b$  (closed circle), and that just out side of the mirror throat  $\Phi_{WI}$  (downward triangle). Data during the plug ECRH taken from several shots with similar parameters are shown.

dimensional potential profile measured at the barrier mid plane becomes almost axisymmetric with the heating configuration shown in Fig. 1 [32]. The potentials at the central cell and at the plug have hill profiles while that just outside the mirror throat ( $\Phi_{WI}$ ) has a hollow profile. The potential is also hollow at the end plate. We measure the potentials in reference to the vacuum vessel. As shown in Fig. 4,  $\Phi_c$  does not vary very much with  $P_{ECRH}$ . The value of  $\Phi_c$  is largely determined by a process inherent to the central cell that is a main plasma source. On the contrary, the potentials at other positions are mainly determined from the axial flux balance on each magnetic field line and the radial profiles as shown in Fig. 5 are observed.

The structure of a thermal barrier and a plug potential can be sustained for 0.15s [33]. This duration is limited by the capacity of the power supply of gyrotrons. The values of  $\phi_c$  and  $\phi_b$  are almost constant for this duration and no indication of barrier filling is seen. The duration of 0.15s is longer than the barrier filling time predicted by the Fuch Lodestro formula of about 30ms. This means that there is a process of natural barrier pumping.

#### 4.2 Current Flow in GAMMA 10

As shown in Figs. 6 (b) and (c), on application of the plug ECRH, the axial ion flux is strongly plugged and at the same time a large electron flux is observed at the end plate. This electron flow is a key factor of the

potential. The temperature of the electron flow also increases with ECRH. The electron flow usually consists of two components with different temperatures  $T_L$  and  $T_H$ . An effective temperature defined as  $T_{\text{eff}} = (1 - \beta)T_L + \beta T_H$  well represents the mean energy of the electron flow, where  $\beta$  is the flux ratio of the  $T_H$  component to the total flux at the end plate.

The potential differences  $\Delta\Phi$  between each position along a magnetic field line increase with  $P_{\text{ECRH}}$  as shown in Fig. 4. The potential differences  $\Phi_P - \Phi_{\text{EP}}$  and  $\phi_{\text{pb}} = \Phi_P - \Phi_B$  are plotted as functions of  $T_{\text{eff}}$  in Fig. 7. Both the potential differences linearly increase with  $T_{\text{eff}}$  and hence  $\Delta\Phi/T_{\text{eff}}$  is nearly constant. This means that  $\Phi_P$  is connected with  $\Phi_{\text{EP}}$ . Therefore,  $\Phi_P$  is indirectly affected by the process that determines  $\Phi_{\text{EP}}$ . Similarly,

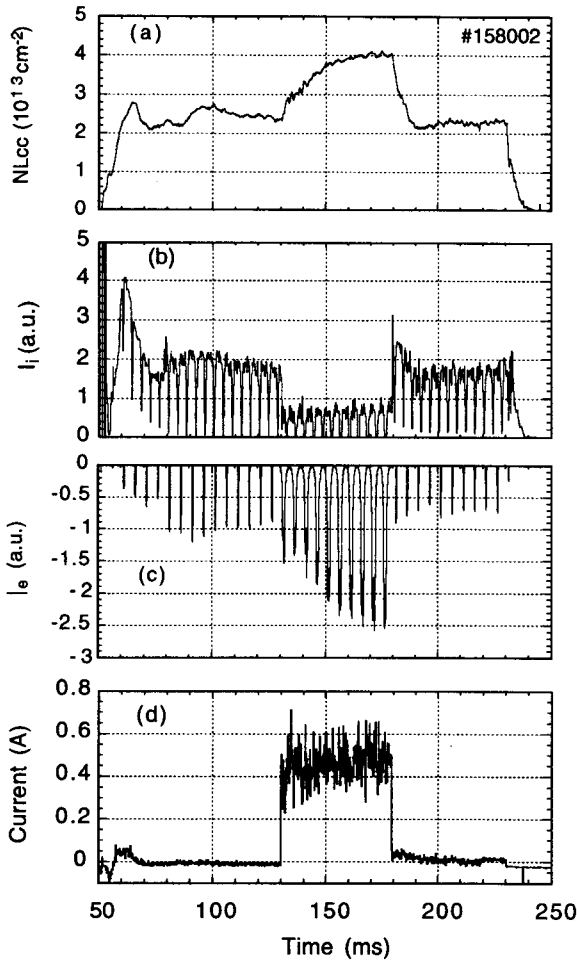


Fig. 6 Typical wave forms are shown of the line density in the central cell (a), the end loss ion current (b), the end loss electron current (c) and the current detected on an electrode in the end mirror cell (d). Pulse trains in Figs. (b) and (c) are due to the sweep of the repeller voltage for energy analysis.

$\phi_{\text{pb}}$  is determined by the plug ECRH-driven warm electron flow while the barrier depth  $\phi_b = \Phi_C - \Phi_B$  scales with the bulk electron temperature [34]. In this sense the barrier depth  $\phi_b$  certainly isolates the warm electrons from the bulk electrons in the central region.

The axial electron flow is also closely connected with an ion flow across magnetic field lines. Figure 6 (d) shows an ion current detected during the plug ECRH on an electrode in the end mirror cell. Figure 8 plots the ion currents as functions of the axial electron flux. After step wise increases with application of the plug ECRH, the ion currents on each electrode increase with the axial electron flux. Since the flux-mapped diameters of the electrodes are larger than the diameter of the central cell limiter, the observed ion currents indicate radial transport of a plasma in the end mirror cell. We measure a net current on each electrode as a sum of an ion current, an electron current and possibly a secondary electron current. During the plug ECRH, a net ion current is detected on the electrodes. Figure 8 indicates that the electron current flowing into the end plate is connected through the metal vacuum vessel with the ion currents on the electrodes. Detailed analysis of the ion currents is published elsewhere [35].

#### 4.3 Dynamic Feature of Potential Formation in the End Mirror Cell

We have measured the axial potential distribution in the end mirror cell in detail. Figure 9 plots the potential distributions with and without the plug ECRH. The on-axis ( $r_c = 0\text{cm}$ ) value of  $\Phi_C$  and  $\Phi_B$  are

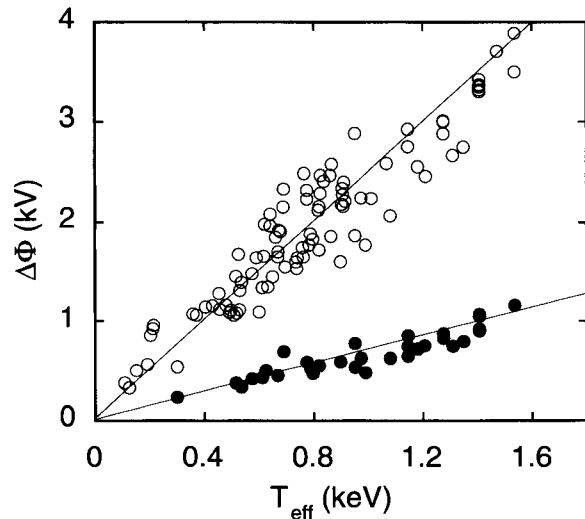


Fig. 7 The potential differences  $\Phi_P - \Phi_{\text{EP}}$  (open circle) and  $\phi_{\text{pb}} = \Phi_P - \Phi_B$  (closed circle) are plotted as functions of the mean temperature  $T_{\text{eff}}$  of the axial warm electron flux.

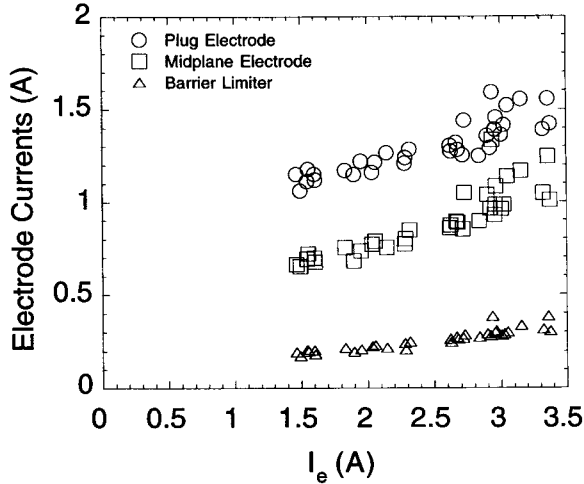


Fig. 8 The ion currents on the electrodes are plotted as functions of the axial electron flux.

measured by beam probes. The potentials  $\Phi_{MT}$  at the mirror throat and  $\Phi_{WI}$  outside the mirror throat are measured by Langmuir probes inserted into the equivalent radius  $r_c = 4.6\text{cm}$ . The plug potential  $\Phi_P$  without ECRH is measured by a Langmuir probe inserted to  $r_c = 0\text{cm}$  at the axial position of  $B = 1\text{T}$ . With ECRH,  $\Phi_P$  is evaluated with an end loss particle analyzer. By using a short pulse ECRH (10 – 20ms), we have confirmed that the Langmuir probe reads almost the same value as the potential from the end loss analyzer.

First we examine the potential distribution without the plug ECRH (denoted by open symbols). The potential has a minimum value at the mid plane. It increases with the magnetic field strength and attains to a maximum at the outer mirror throat. Then, it again decreases outside the mirror throat. The end plate potential is about  $-110\text{V}$ . The plasma is produced in the central cell and flows out along magnetic field lines to the end. The electron density of the flow plasma becomes minimum at the mid plane of the end mirror cell and again increases toward the outer mirror throat. The measured axial potential distribution corresponds to this picture. The potential difference  $\phi_b = \Phi_C - \Phi_B = 260\text{V}$  normalized by the electron temperature is five through six. This is on the  $\phi_b - T_e$  scaling [34]. Since the barrier density is about 1/15 times as large as that at the central cell, the potential difference expected from the Boltzmann's law is less than 150V. Under the presence of a finite plasma flow, the inertia term of the momentum balance equation is not negligible and the Boltzmann's law does not necessarily hold.

With the plug ECRH, the potential distribution

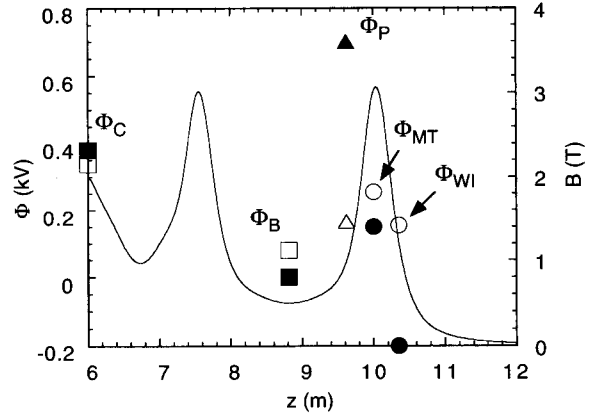


Fig. 9 The axial potential distributions in the end mirror cell are shown. The open symbols denote the potentials without the plug ECRH and the closed symbols stand for those during the plug ECRH.  $\Phi_C$  is plotted expediently at  $z = 6\text{m}$ .

(plotted by the closed symbols) drastically varies. Potential data taken from a plasma shot of  $P_{ECRH} = 130\text{kW}$  are plotted in Fig. 9. The potential  $\Phi_P$  at the plug drastically increases and consequently  $\phi_{pb}$  attains to 700V. The barrier depth  $\phi_b$  also increases but  $\phi_c = \phi_{pb} - \phi_b$  of a positive value is generated. The potentials  $\Phi_{MT}$  and  $\Phi_{WI}$  at the positions outside the plug substantially decrease. The end plate potential goes down to  $-1600\text{V}$ . As shown in Fig. 10, while the electron density at the mid plane inside the plug potential increases (Fig. (a)), the electron density just outside the plug decreases as a result of plugging (Fig. (b)). The density distribution is not static but changes dynamically with the potential. The large decreases in  $\Phi_{WI}$  and  $\Phi_{EP}$  stem from the warm electron flow [5,25].

## 5. Discussion

### 5.1 Improvement of Plasma Confinement

Plasma confinement is improved by potential formation [3]. Figure 11 stands for the time variation of the on-axis value of the central cell electron density. As shown in Fig. 5, the ion confining potential  $\phi_c = \Phi_P - \Phi_C$  is formed within the radius  $r_c \leq 7\text{cm}$  that is largely determined by the radiation pattern of the plug ECRH on the resonance surface. Therefore, confinement within this radius is improved. The plasma density near the axis increases and it doubles with potential formation. The large increase in the central cell density has been realized after modification of the plug ECRH antenna system for axisymmetric heating [22]. The enhancement factor strongly depends on the axisymmetry of the potential. So, further reduction of residual asymmetry of

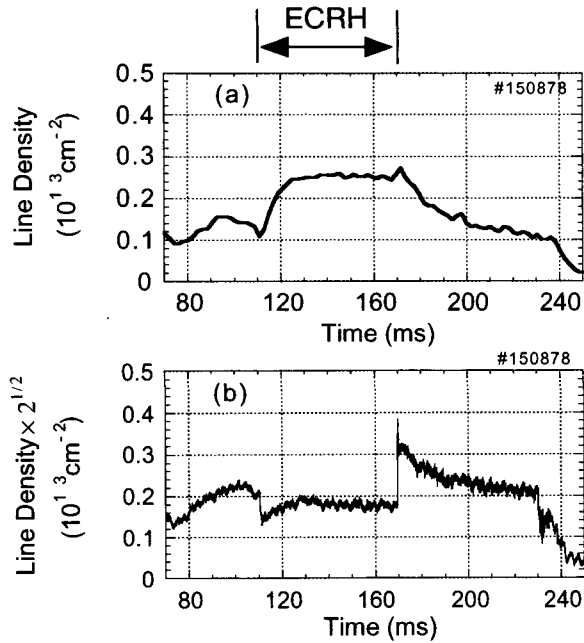


Fig. 10 Time variations are shown of (a) the line densities at the barrier mid plane ( $B = 0.5T$ ) and (b) at a position just outside the plug region ( $B \geq 1.0T$ ). To be comparable as a density, the line density at the plug region is multiplied by  $2^{1/2}$ .

heating is necessary. The maximum density so far obtained during potential formation is  $4 \times 10^{12} \text{cm}^{-3}$ .

Particle confinement is examined using a particle balance study. The ionization source current is evaluated from combination of  $H_{\alpha}$  emissivity measurement with a calibrated detector array and calculation with the DEGAS code [36]. The particle confinement time of the plasma within  $r_c \leq 7\text{cm}$  increases from less than 10ms to 40 through 50ms by potential formation [3].

## 5.2 Discussion on Potential Formation

Katanuma et al. have presented a new scheme of potential formation [6,7]. The potential maximum is formed at the outer mirror throat for a flow plasma. This corresponds to the case of no ECRH, as plotted by the open symbols in Fig. 9. The scheme shows that the plug ECRH breaks the symmetry of the flow plasma with respect to the mid plane of the end mirror cell and  $\Phi_p$  higher than  $\Phi_c$  is generated at a position inside the mirror throat. However, effects of ECRH are introduced indirectly and the axial position of the plug should be determined from the balance between the action of ECRH on electrons and the ion reflection by the plug potential. A recent basic experiment has shown that a plug potential can be formed with fundamental ECRH alone [8,9]. ECRH enhances mirror-reflection of

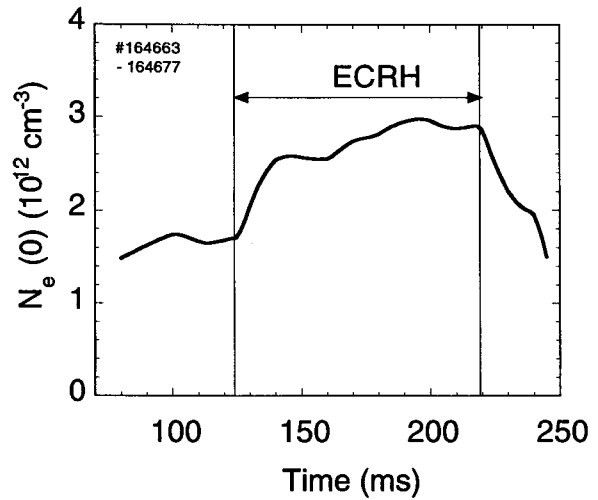


Fig. 11 An example of the time variation of the on-axis density in the central cell is shown.

electrons in a flow plasma. Then an excess positive charge is left downstream, which results in a positive potential. The ion flux is reflected by this potential and consequently charge neutrality is kept. This experiment provides many indications to the GAMMA experiment. However, plasma confinement in the basic experiment is poor and the situations at the steady state may be different. In GAMMA 10, moreover, an intense warm electron flow has an important role.

The experimental observations strongly suggest the importance of global point of view. The potentials at each position, expressed by capital  $\Phi$ 's are measured in reference to the potential of the vacuum vessel ( $\Phi = 0V$ ). In the axial motion, particles feel only the potential differences along a magnetic field line such as  $\phi_c$  or  $\phi_b$ . However,  $\Phi$ 's should have a physical meaning, particularly when we consider the three-dimensional potential structure. The value of each  $\Phi$  is determined from self-consistency between the axial and the radial particle transport. For example, the weak response of  $\Phi_c$  to the plug ECRH power implies a radial transport intrinsic to the central cell. Experiments show that the plug potential exists near the axial position with  $B = 1.0T$  but its exact position has not been pointed out. It should be determined from the balance between the action of ECRH on electrons and the ion reflection by the plug potential. Moreover, radial losses may enhance the plug potential as predicted by Hojo et al. [37,38]

The global point of view is particularly important in the linkage of  $\Phi_p$  to  $\Phi_{EP}$ . The warm electron flow connects  $\Phi_p$  to  $\Phi_{EP}$  as indicated in Fig. 7. Thus the processes that determine the value of  $\Phi_{EP}$  are closely

related to  $\Phi_p$ . Experimentally,  $\Phi_{EP}$  is not determined by only a simple condition to be electrically floating but a finite net current through the end plate is also a non-negligible factor of  $\Phi_{EP}$ . A series of experiments of mesh bias suppressing the secondary electrons from the end plate [29,30] and variation of the end plate resistance [39] has revealed this point. The net current is connected to the ion currents on the electrodes in the end mirror cell [35]. The value of  $\Phi_{EP}$  increases with the net current and consequently  $\Phi_p$  does. On the other hand,  $\Phi_p$  is not very tightly linked to  $\Phi_C$ . Thus, the value of  $\Phi_{EP}$  can affect the magnitude of the confining potential  $\phi_c$ . We have not adequately understood the potential physics in the end region yet and continuous efforts to full understanding of it are necessary.

## 6. Conclusions

Experimental observations on the potential formation in the GAMMA 10 tandem mirror are presented. Fundamental ECRH at the plug region (plug ECRH) plays a largest role in the potential formation. On application of the plug ECRH, the axial and radial potential structures show significant changes. The density distribution of the ions near the plug region is not invariant but strongly modified by plugging corresponding to the potential profile. An intense axial flow of warm electrons driven by the plug ECRH has a key role of the potential distribution. The potential difference between the plug and the barrier mid plane increases with the temperature of the warm electrons. The warm electron flow also predominantly determines the potential distribution in the end region located outside the plug. Although a substantial improvement of plasma confinement by potential is realized, there still remain many issues for further improvement of tandem mirror plasma confinement.

## References

- [1] S. Miyoshi *et al.*, Nucl. Fusion **30**, 1761 (1990).
- [2] M. Inutake *et al.*, Phys. Rev. Lett. **55**, 939 (1985).
- [3] Yatsu *et al.*, Nucl. Fusion **39**, 1707 (1999).
- [4] D.E. Baldwin, ed., Physics Basis for MFTF-B UCID-18496 (1980).
- [5] K. Kurihara *et al.*, J. Phys. Soc. Jpn. **61**, 3153 (1992).
- [6] I. Katanuma *et al.*, Phys. Plasmas **3**, 2218 (1996).
- [7] I. Katanuma *et al.*, Phys. Plasmas **5**, 1560 (1998).
- [8] T. Kaneko *et al.*, Phys. Rev. Lett. **80**, 2602 (1998).
- [9] T. Kaneko *et al.*, J. Phys. Soc. Jpn. **69**, 2060 (2000).
- [10] R.F. Post, Nucl. Fusion **27**, 1579 (1987).
- [11] V.P. Pastukhov, Nucl. Fusion **14**, 3 (1974).
- [12] G.I. Dimov *et al.*, Sov. J. Plasma Phys. **2**, 326 (1976).
- [13] T.K. Fowler *et al.*, Comments on Plasma Phys. and Control. Fusion **2**, 167 (1977).
- [14] R.H. Cohen *et al.*, Nucl. Fusion **18**, 1229 (1978).
- [15] S. Miyoshi *et al.*, 7th Int. Conf. Plasma Physics Control. Nucl. Fusion Res., Innsbruck, 1979, Vol.II, 437.
- [16] F.H. Coensgen *et al.*, Phys. Rev. Lett. **44**, 1132 (1980).
- [17] D.E. Baldwin *et al.*, Phys. Rev. Lett. **43**, 1318 (1979).
- [18] T.C. Simonen *et al.*, Phys. Rev. Lett. **50**, 1668 (1983).
- [19] R.S. Post *et al.*, Proc. of the 11th Int. Conf. Plasma Phys. Control. Nucl. Fusion Res., Kyoto, 1986, Vol.II, p251.
- [20] R.H. Cohen *et al.*, Nucl. Fusion **20**, 1421 (1980).
- [21] R.H. Cohen, Phys. Fluids **26**, 2774 (1983).
- [22] T. Saito *et al.*, Fusion Engineering and Design **53**, 267 (2001).
- [23] K. Ishii *et al.*, Rev. Sci. Instrum. **60**, 3270 (1989).
- [24] Y. Sakamoto *et al.*, Rev. Sci. Instrum. **66**, 4928 (1995).
- [25] Y. Yoshimura *et al.*, J. Phys. Soc. Jpn. **66**, 3461 (1997).
- [26] M. Ichimura *et al.*, Nucl. Fusion **39**, 1995 (1999).
- [27] T. Saito *et al.*, Phys. Fluids **B5**, 866-871 (1993).
- [28] Y. Tatematsu *et al.*, J. Phys. Soc. Jpn. **63**, 558 (1994).
- [29] T. Saito *et al.*, Phys. Plasmas **2**, 352 (1995).
- [30] K. Kajiwara *et al.*, J. Phys. Soc. Jpn. **66**, 2342 (1997).
- [31] Y. Tatematsu *et al.*, presented in this conference.
- [32] N. Kikuno *et al.*, Rev. Sci. Instrum. **70**, 4251 (1999).
- [33] K. Yatsu *et al.*, 18th IAEA Fusion Energy Conference, IAEA-CN-77/EXP1/10.
- [34] T. Cho *et al.*, 18th IAEA Fusion Energy Conference, IAEA-CN-77/EXP5/10.
- [35] K. Kajiwara *et al.*, J. Phys. Soc. Jpn. **70**, 421 (2001).
- [36] S. Kobayashi *et al.*, J. Nucl. Materials **266-269**, 566 (1999).
- [37] H. Hojo, J. Phys. Soc. Jpn. **62**, 4148 (1993).
- [38] H. Hojo *et al.*, J. Phys. Soc. Jpn. **64**, 3610 (1995).
- [39] T. Saito *et al.*, Trans. Fusion Technology **39**, 143 (2001).